Journal of Biomedical Optics

BiomedicalOptics.SPIEDigitalLibrary.org

Development of human serum albumin conjugated with near-infrared dye for photoacoustic tumor imaging

Kengo Kanazaki
Kohei Sano
Akira Makino
Atsushi Takahashi
Jun Deguchi
Manami Ohashi
Takashi Temma
Masahiro Ono
Hideo Saji

SPIE.

Development of human serum albumin conjugated with near-infrared dye for photoacoustic tumor imaging

Kengo Kanazaki,[a] Kohei Sano,[b,c] Akira Makino,[b,d] Atsushi Takahashi,[a] Jun Deguchi,[b] Manami Ohashi,[b] Takashi Temma,[b] Masahiro Ono,[b] and Hideo Saji[b,*]
[a]Canon Inc., Medical Imaging Project, Corporate R&D Headquarters, 3-30-2 Shimomaruko, Ohta-ku, Tokyo 146-8501, Japan
[b]Kyoto University, Department of Patho-Functional Bioanalysis Graduate School of Pharmaceutical Sciences, 46-29 Yoshida Shimoadachi-cho, Sakyo-ku, Kyoto 606-8501, Japan
[c]Kyoto University Hospital, 54 Kawaharacho, Shogoin, Sakyo-ku, Kyoto 606-8507, Japan
[d]University of Fukui, Biomedical Imaging Research Center, 23-3 Matsuokashimoaizuki, Eiheiji-cho, Yoshida-gun, Fukui 910-1193, Japan

Abstract. Photoacoustic (PA) imaging has emerged as a noninvasive diagnostic method which detects ultrasonic waves thermoelastically induced by optical absorbers irradiated with laser. For tumor diagnosis, PA contrast agent has been proposed to enhance the PA effect for detecting tumors sensitively. Here, we prepared a human serum albumin (HSA) conjugated with indocyanine green (ICG) as a PA contrast agent allowing enhanced permeability and retention effect for sensitive tumor imaging. The feasibility of PA imaging with HSA-ICG to detect allografted tumors was evaluated in tumor-bearing mice. *In vivo* fluorescence imaging and radiolabeled biodistribution study showed that the biodistribution dramatically changed as the number of ICG bound to HSA increased, and the maximum accumulation of ICG was achieved when around three ICG molecules were loaded on an HSA. *In vivo* PA imaging demonstrated a tumor-selective and dose-dependent increase of PA signal intensity in mice injected with HSA-ICG ($R^2 = 0.88$, 387% increase for HSA-ICG, 104 nmol ICG). In conclusion, HSA-ICG clearly visualized the allografted tumors with high tumor-to-background ratios having high quantitative and spatial resolution for the sensitive PA imaging of tumors. HSA-ICG could be useful as a favorable contrast agent for PA tumor imaging for the management of cancer. [DOI: 10.1117/1.JBO.19.9.096002]

Keywords: human serum albumin; indocyanine green; cancer; photoacoustic imaging.

Paper 140207RR received Mar. 31, 2014; revised manuscript received Aug. 9, 2014; accepted for publication Aug. 12, 2014; published online Sep. 5, 2014.

1 Introduction

In recent years, photoacoustic (PA) imaging (PAI) has emerged as a new type of hybrid biomedical diagnostic method.[1,2] PAI noninvasively detects ultrasonic waves thermoelastically induced by the absorption of photons by biomolecules through the PA effect, and these ultrasonic waves are scattered much less than photons. The detailed mechanism is as follows: (1) a body is irradiated with a nonionizing nanosecond-pulsed laser beam, (2) as the light spreads and diffuses into the body, it is differentially absorbed by the various regions of the tissues, (3) the light absorption briefly increases the temperature of the tissue, (4) this increases the pressure in proportion to the amount of absorbed light energy, thus generating sound waves, (5) the sound waves can be measured by ultrasonic transducers, and then reconstructed into an image of optical absorption by computer algorithms. PAI can provide anatomical and functional information with high resolution by probing a wide variety of endogenous absorbers including hemoglobin, melanin, and water. Recently, a small animal PA imaging system to detect the tumor vasculature has been developed.[3] On the other hand, exogenous PA contrast agents further extend PAI to molecular imaging.[4] Organic dyes[5,6] and nanoparticles[7] can serve as excellent PA contrast agents. Among them, indocyanine green (ICG) has been used for tumor imaging by delivery of nanocarrier encapsulated ICG molecules,[8,9] because it shows an absorption in the near-infrared (NIR) window where the optical window permits photons to penetrate into biological tissues with a relatively high transmittance.[10] Although ICG has long been approved by the Food & Drug Administration (FDA) for human use in retinal angiography and for intraoperative assessment of liver function,[11,12] the clinical translation of most nanoparticles is still awaiting FDA approval. Therefore, clinical-use PA contrast agents for tumor imaging are strongly desired.

Human serum albumin (HSA) is a blood protein and is attracting attention as a drug carrier,[13] such as for Abraxane® (albumin-bound paclitaxel for injectable suspension).[14] The combination of low molecular weight drugs and water-soluble high molecular weight molecules such as HSA seems to promote the uptake of drugs in the tumor *via* enhanced permeability and retention (EPR) effects.[15,16] In this paper, we prepared a HSA conjugated with ICG as a PA contrast agent for the diagnosis of cancer, and its feasibility for PA tumor imaging was evaluated *in vivo* in tumor-bearing mice.

2 Materials and Methods

2.1 *Reagents*

HSA was purchased from Sigma Aldrich (St. Louis, Missouri). 2-[7-[1,3-Dihydro-1,1-dimethyl-3-(4-sulfobutyl)-2H-benzo[e] indol-2-ylidene]-1,3,5-heptatrienyl]- 1,1-dimethyl-3-[5-(3-

*Address all correspondence to: Hideo Saji, E-mail: hsaji@pharm.kyoto-u.ac.jp

sulfosuccinimidyl)oxycarbonylpentyl]-1H-benzo[e]indolium, inner salt, sodium salt (ICG-Sulfo-OSu) was purchased from Dojindo Molecular Technologies, Inc. (Kumamoto, Japan). 2-(4-Isothiocyanatobenzyl)-diethylenetriaminepentaacetic acid (*p*-SCN-Bn-DTPA) was purchased from Macrocyclics Inc. (Dallas, Texas). $^{111}InCl_3$ (74 MBq/mL in 0.02 N HCl) was purchased from Nihon Medi-Physics (Tokyo, Japan). Intralipid fluid solution 20% was purchased from Fresenius Kabi Japan (Tokyo, Japan). All other chemicals used were of the highest purity available.

2.2 *Cell Culture*

Colon26, a mouse cell line derived from rectal cancer, was purchased from Riken Bio Resource Center (Ibaraki, Japan). The cells were maintained in Dulbecco's modified Eagle's medium (Life Technologies Co., Carlsbad, California) supplemented with 10% heat-inactivated fetal bovine serum (Life Technologies Co.), 100 U/ml penicillin, and 100 μg/ml streptomycin in a 5% CO_2/air incubator at 37°C.

2.3 *Preparation of Human Serum Albumin-Indocyanine Green*

HSA [10 mg in 1-ml carbonate buffer (pH 8.5)] was mixed with ICG-Sulfo-OSu (10.8 mM in DMSO) at the ratio of HSA : ICG = 1 : 1, 1 : 7, and 1 : 21, respectively. The mixed solutions were incubated at room temperature for 3 h, and then purified by diafiltration membrane (Amicon Ultra Centrifugal Filter Unit (nominal molecular weight limit is 30 kDa), Millipore Co., Darmstadt, Germany) with PBS. The sizes of HSA-ICG and HSA were measured by dynamic light scattering using the Zetasizer Nano ZS series (Malvern Instruments Ltd., Worcestershire, UK) at 25°C. The molecular weights of the purified samples were analyzed by sodium dodecyl sulfate polyacrylamide gel electrophoresis (SDS-PAGE, Novex® Tris-Glycine 4–20% gel, Life Technologies Co.) stained by Coomassie Brilliant Blue (CBB). The covalent and noncovalent fractions of ICG bound to HSA were also assessed by SDS-PAGE, where each HSA-ICG (10 pmol ICG) and ICG-Sulfo-OSu (0–40 pmol) was electrophoresed (90 min) and the fluorescence intensity of ICG-Sulfo-OSu itself and that of unbound ICG of HSA-ICG in the gel were measured with a fluorescence imaging system (IVIS imaging System 200, Perkin Elmer Inc., Waltham, Massachusetts). The noncovalent fraction of ICG bound to HSA was calculated by a standard curve obtained by plotting the fluorescence intensity against the concentration of ICG-Sulfo-OSu in order to determine the chemical purity. The protein concentration was determined by BCA assay (Thermo Fisher Scientific Inc., Waltham, Massachusetts). The concentration of ICG of HSA-ICG was measured by absorption in the presence of 5% SDS with the UV-Vis-NIR system (UV-1800, Shimazu Co., Kyoto, Japan) to confirm the number of fluorophore molecules conjugated to HSA. To evaluate the stability of each HSA-ICG, each conjugate was mixed with mouse blood plasma (1 : 9, v/v) and incubated for 24 h at 37°C. The mixture was analyzed by SDS-PAGE.

2.4 *Animal Model*

Animal studies were conducted in accordance with the institutional guidelines of Kyoto University, and the experimental procedures were approved by the Kyoto University Animal Care Committee. Five-weeks-old female BALB/c-nu/nu nude mice were purchased from Japan SLC (Shizuoka, Japan). The total number of mice used in these animal experiments was 110. The animals were housed in air-conditioned rooms under a 12-h light/dark cycle and allowed free access to food and water. Colon26 (1×10^6 cells) suspended in each 50 μl of PBS was inoculated subcutaneously in the shoulder and leg region of the mice. Experiments with tumor-bearing mice were performed 7 days after inoculation.

2.5 *In Vitro Measurement of Photoacoustic Signals*

The setup for the PA signal measurement system consisted of pulsed light of wavelength 797 nm generated by the Model Titanium Sapphire Laser system (Lotis TII, Minsk, Belarus) operating at 10 Hz with a 20-ns pulse duration. A transducer Model V303 (Panametrics-NDT, Waltham, Massachusetts) (1-MHz center frequency, 1-cm element size) and ultrasonic preamplifier Model 5682 (Olympus Corporation, Tokyo, Japan) collected the PA signal. DPO3034 (Tektronix Company, Tokyo, Japan) was used as a gauge and light detection by a photodiode as a trigger.

2.6 *Evaluation of In Vivo Tumor Uptake of Human Serum Albumin-Indocyanine Green by Fluorescence Measurement*

To estimate the tumor accumulation of HSA-ICGs, each HSA-ICG or ICG not bound to HSA (13 nmol ICG) was suspended in 100-μl PBS and injected into the tail vein of colon26 tumor-bearing nude mice ($n = 3$ for each probe at each time point). For each sample, 1, 6, and 24 h after i.v. injection of HSA-ICGs, whole-body fluorescence images were acquired using the IVIS imaging System 200 (ex: 745 nm, em: 840 nm, exposure time: 1 s). After all scans, the tumors were excised and homogenized by adding 1% triton-X aqueous solution. The tumor homogenate was centrifuged at 16,000 g for 5 min at 4°C, and the supernatant was collected. The supernatant (2 μl) was mixed with DMSO (18 μl), and the fluorescence intensity was measured. The HSA-ICG concentration in tumor homogenates was calculated by using a standard curve prepared by HSA-ICG ($0.0625 - 4$ μM) diluted with mouse tumor homogenate. To evaluate the influence of injection dose on tumor accumulation of HSA-ICG2.9, a high dose of HSA-ICG2.9 (104-nmol ICG) was administered to the colon26 tumor-bearing mice ($n = 3$) and tumor uptake was investigated as above. Fluorescence intensity was calculated by setting regions of interest manually drawn on tumors and muscle, and tumor-to-background (muscle) ratios were calculated.

2.7 *Biodistribution of Radiolabeled Human Serum Albumin-Indocyanine Green*

p-SCN-Bn-DTPA dissolved into phosphate buffer (0.1 M, pH 8.6) was added to HSA-ICG or HSA in a molar ratio of $0.7 - 2.0 : 1$. The mixture was incubated for 6 h at 37°C under protection from light. After purification by a diafiltration membrane (30 kDa) with phosphate buffer (0.1 M, pH 8.6), DTPA-HSA-ICG was obtained. The number of DTPAs conjugated to HSA-ICGs and HSA was adjusted to 0.5. DTPA-HSA-ICG was mixed with $^{111}InCl_3$ in 0.1 M-sodium acetate (pH 6.0) followed by incubation for 15 min at room temperature. The buffer exchange was performed by a diafiltration membrane

(30 kDa) with PBS before injection. Radiochemical purity was calculated using PD-10 Columns (GE Healthcare UK Ltd., Buckinghamshire, UK) and diafiltration membrane (30 kDa). ^{111}In-labeled HSA-ICG (37 kBq, 13-nmol ICG/150 μl PBS) or ^{111}In-labeled HSA (37 kBq, 26-nmol HSA/150 μl PBS) was injected into the colon26 tumor-bearing mice *via* the tail vein and the biodistribution was monitored at 1-, 6-, and 24-h postinjection ($n = 3$–4 for each probe at each time point). Organs of interest were excised, weighed, and radioactivity counts were determined with an NaI well-type scintillation counter (1470WIZARD, PerkinElmer Co.) using the injected dose as a standard. Data were calculated as the percentage injected dose per gram of tissue (% ID/g).

2.8 *In Vivo Photoacoustic Imaging*

PA imaging was performed with an Endra Life Sciences Nexus 128 instrument (Endra Inc., Ann Arbor, Michigan). The system is equipped with an optical parametric oscillator tunable laser and 128 transducers arranged on a hemispherical bowl. A plastic tray is placed on top of the bowl for animal positioning. One scan used 120 angles and 100 pulses per angle. The excitation wavelength was 797 nm based on the absorption peak of HSA-ICG. Pulse laser intensity, pulse width, and pulse frequency were 9–11 mJ, 7 nsec, and 20 Hz, respectively. HSA-ICG2.9 (13-, 26-, 52-, and 104-nmol ICG) was injected into the colon26 tumor-bearing mice *via* the tail vein ($n = 3$). PA images were taken before and 24 h after injection. PA images were constructed by volumetric rendering *via* Osirix software. PA signal intensity was calculated from values of volumetric rendering points and were normalized with irradiated laser intensity. Moreover, HSA-ICG0.5, HSA-ICG2.9, and HSA-ICG8.2 (9-nmol HSA) were injected into the mice, and the PA images were acquired under the same conditions mentioned above.

2.9 *Comparison between Photoacoustic Imaging and Fluorescence Imaging*

The intralipid gel was prepared as reported previously.[17] Agarose (0.5%) was dissolved in distilled deionized water by heating to about 90°C. After the temperature fell to 60°C, 1% of intralipid was added to the solution followed by gelation by cooling. The tumors ($n = 3$) excised from colon26 tumor-bearing mice injected with HSA-ICG probes were covered with intralipid gel, and fluorescence images and PA images were acquired using the IVIS imaging System 200 and the Nexus 128 instrument, respectively. The apparent size of a tumor was calculated from the half-value width of the maximum signal intensity. The true sizes of the tumors were measured with a caliper.

2.10 *Statistical Analysis*

Each experiment was individually performed at least three times. In *in vivo* studies, $n = 3$–6 mice were used for each probe at each time point. The statistical significance among groups was identified using the Student's *t*-test (two-tailed). Data are presented as the mean ± standard deviation. *P* values of less than 0.05 were considered statistically significant.

3 Results

3.1 *Preparation of Human Serum Albumin-Indocyanine Green*

As the reaction ratios of ICG-Sulfo-OSu to HSA increased, the number of ICG covalently bound to HSA increased, which are referred to as HSA-ICG0.5, HSA-ICG2.9, and HSA-ICG8.2, sequentially, based on the number of ICG molecules incorporated (Table 1). The size of HSA-ICG increased as the number of ICG bound to HSA increased (6.0 ± 1.2, 7.7 ± 0.7, 8.7 ± 1.7, and 10.4 ± 1.3 nm for HSA, HSA-ICG0.5, HSA-ICG2.9, and HSA-ICG8.2, respectively). The HSA-ICGs preparations showed a strong association between HSA and ICG, and exhibited a slight increase in molecular weight depending on the number of ICG bound to HSA, but there were no detectable HSA aggregates as determined by SDS-PAGE [Fig. 1(a)]. In the fluorescence analyses in SDS-PAGE, high purities (≈90%) were observed for each HSA-ICG [Fig. 1(b)]. In mouse plasma, 99% of HSA-ICG0.5, 94% of HSA-ICG2.9, and 89% of HSA-ICG8.2 were observed as an intact form at 24 h after incubation, which indicated the high stability of HSA-ICG conjugates in mouse plasma.

The basic PA characteristics of each HSA-ICG and ICG were evaluated (Fig. 2). When bound to HSA, ICG showed a 30–40 nm of red shift for NIR absorption [Fig. 2(a)]. The absorption spectra of each conjugate demonstrated the H-dimer formation with the appearance of a blue-shifted peak, which was

Table 1 Properties of HSA-ICG.

	Mixed rate of ICG-Sulfo-OSu to HSA	D/P	Purity (%)
HSA-ICG0.5	1	0.5	89
HSA-ICG2.9	7	2.9	93
HSA-ICG8.2	21	8.2	89

Note: D/P = (ICG concentration covalently bound to HSA)/(HSA concentration).; Purity = (ICG covalently bound to HSA)/(Total ICG).

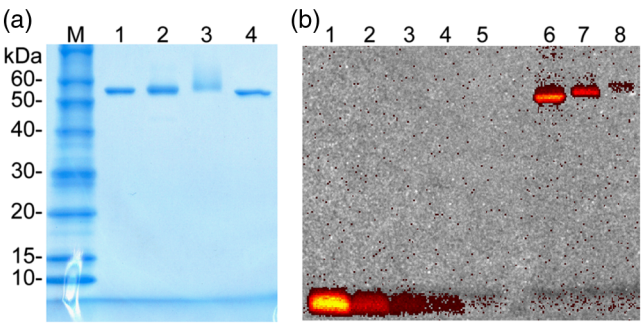

Fig. 1 Electrophoretic analysis of human serum albumin-Indocyanine green (HSA-ICG). (a) The gel stained by CBB to detect HSA. Lane M, molecular weight marker; 1, HSA-ICG0.5; 2, HSA-ICG2.9; 3, HSA-ICG8.2; 4, HSA. (b) Fluorescence images of ICG-Sulfo-OSu and HSA-ICG after electrophoresis. 1, ICG-Sulfo-OSu 40 pmol; 2, ICG-Sulfo-OSu 20 pmol; 3, ICG-Sulfo-OSu 10 pmol; 4, ICG-Sulfo-OSu 5 pmol; 5, ICG-Sulfo-OSu 2.5 pmol; 6, HSA-ICG0.5; 7, HSA-ICG2.9; 8, HSA-ICG8.2.

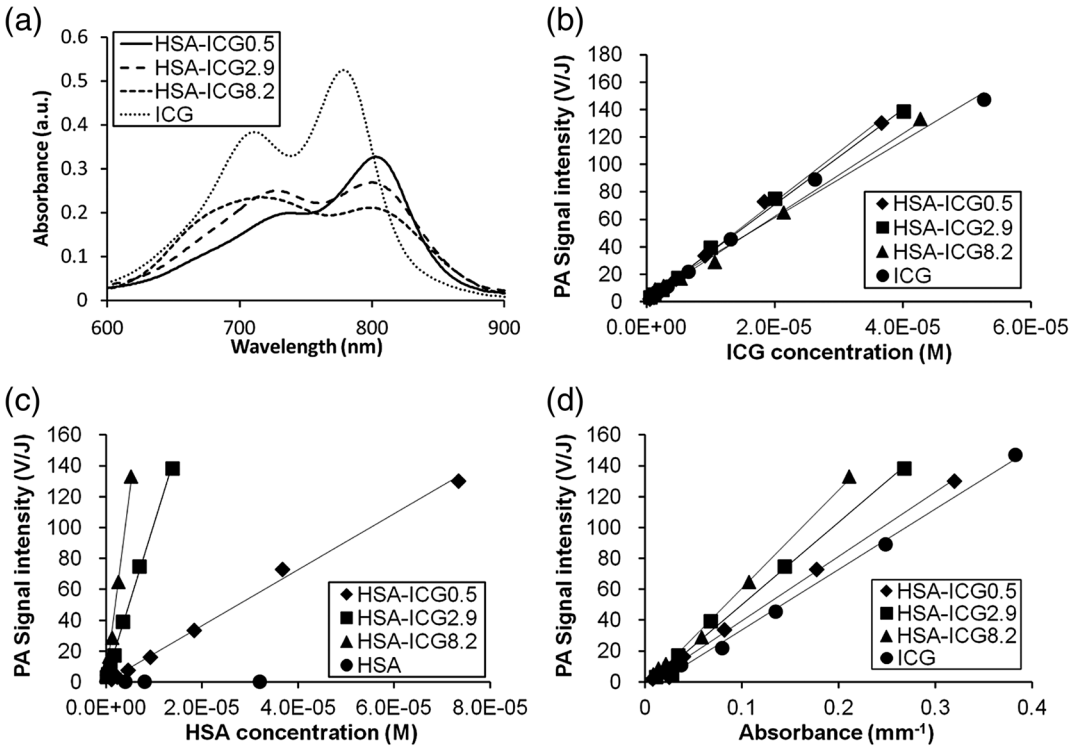

Fig. 2 Absorption spectra and PA signals of HSA-ICG. (a) Near-infrared (NIR) absorption spectra of ICG and HSA-ICG. The ICG concentration of each sample was approximately 4 μM. (b)–(d) PA signal plotted against ICG concentration, HSA concentration, and absorbance value, respectively.

remarkable for HSA conjugated with many ICG molecules. The PA signal produced by HSA-ICG was linearly dependent on the ICG concentration, which was comparable to the ICG dye alone [Fig. 2(b)]. The PA signal intensity to HSA concentration was superior in order of HSA-ICG8.2 > HSA-ICG2.9 > HSA-ICG0.5 > HSA in proportion to the number of ICG bound to HSA [Fig. 2(c)]. The relative PA signal intensities to HSA concentration of HSA-ICG were 1, 5.6, and 13.7 for HSA-ICG0.5, HSA-ICG2.9, and HSA-ICG8.2, respectively, which was calculated based on the slope of the PA signal intensity to the HSA concentration [Fig. 2(c)]. Furthermore, the PA signal was plotted against the absorption of 797 nm for each sample [Fig. 2(d)]. Even if the absorption of 797 nm was low, HSA-ICG, which had many ICGs, produced a strong PA signal. Taken together, it was confirmed that not only absorption, but also ICG concentration of HSA-ICG contributed to PA signal intensity.

3.2 *Evaluation of In Vivo Tumor Uptake of Human Serum Albumin-Indocyanine Green by Fluorescence Measurement*

To confirm the tumor accumulation of HSA-ICG, each preparation was injected into colon26 tumor-bearing nude mice, and whole-body fluorescence images were obtained using the *in vivo* fluorescence imager 1, 6, and 24 h after i.v. injection of HSA-ICG (Fig. 3). Tumors were detected for each probe after 6 and 24 h [Fig. 3(a)]. At 24 h after i.v. injection, the fluorescence signal intensity at tumor regions was similar between groups (1.0×10^8, 1.2×10^8, 1.5×10^8 photons/s/cm^2/steradian for HSA-ICG0.5, HSA-ICG2.9, and HSA-ICG8.2, respectively). On the other hand, tumor uptake (%ID/g) at 24 h after i.v. injection decreased with the increase of ICG bound to HSA (17.4, 10.6, and 2.1% ID/g for HSA-ICG0.5, HSA-ICG2.9, and HSA-ICG8.2, respectively), as determined by measuring ICG fluorescence in the tumor homogenates [Fig. 3(b)]. The tumor uptake of ICG not bound to HSA was 0.12 ± 0.02, 0.06 ± 0.01, and 0.02 ± 0.004% ID/g at 1-, 3-, and 24-h post-injection, respectively. Even if the injection dose of HSA-ICG2.9 to the mouse was increased, tumor uptake did not change at 24 h after i.v. injection (10.6 ± 2.6 and 9.3 ± 1.7% ID/g for 13 and 104 nmol, respectively) [Fig. 3(c)]. This result was also applicable for HSA-ICG0.5 and HSA-ICG8.2 (18.3 ± 0.9 and 2.6 ± 0.4% ID/g for HSA-ICG0.5 and HSA-ICG8.2 (104-nmol ICG), respectively). The tumor/muscle fluorescence intensity ratios of HSA-ICG0.5 and HSA-ICG2.9 gradually increased with time. On the other hand, those of HSA-ICG8.2 stayed constant over the entire period [Fig. 3(d)].

3.3 *Biodistribution of Radiolabeled Human Serum Albumin-Indocyanine Green*

The results of *in vivo* biodistribution studies of ^{111}In-DTPA-HSA-ICG (D/P = 0, 0.5, 2.9, and 8.2) at 1, 6, and 24 h are summarized in Table 2. Probe accumulation in the tumor at 24-h postinjection was 16.8, 15.9, 9.5, and 2.9% ID/g for ^{111}In-DTPA-HSA, ^{111}In-DTPA-HSA-ICG0.5, ^{111}In-DTPA-HSA-ICG2.9, and ^{111}In-DTPA-HSA-ICG8.2, respectively, which was in accordance with the results obtained in the *in vivo* fluorescence imaging study [Fig. 3(b)]. As the number of ICG bound to HSA increased, the ICG uptake in the liver was markedly increased coincidentally with the decrease in that of the blood and kidney, probably due to the molecular size

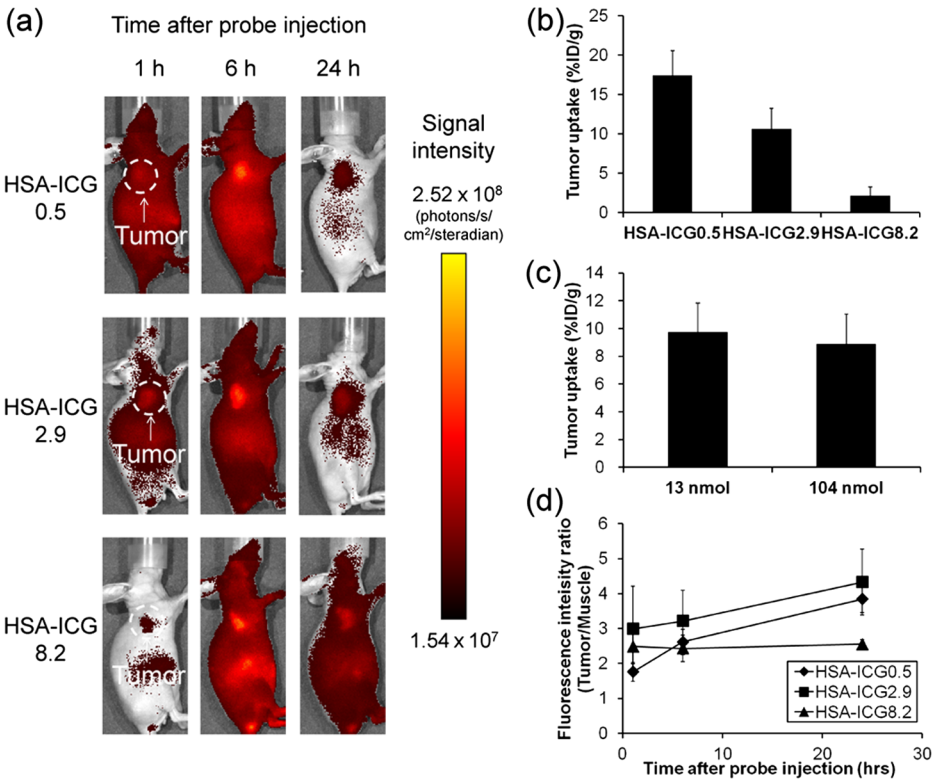

Fig. 3 *In vivo* fluorescence images of tumor-bearing mice injected with HSA-ICG. (a) The whole-body near-infrared (NIR) fluorescence images of mice were acquired at 1, 6, and 24 h after intravenous injection of probes. (b) The uptake of HSA-ICGs (13 nmol) in the tumor at 24 h. (c) The tumor uptake of HSA-ICG2.9 (13 and 104-nmol ICG) at 24 h. (d) The temporal change of fluorescence intensity ratios (Tumor/Muscle) calculated based on whole-body NIR fluorescence images of mice.

and electric charge. Tumor/Blood (T/B) and Tumor/Muscle (T/M) ratios for all HSA-ICGs gradually increased with time. Among them, the highest T/B ratios were obtained for HSA-ICG8.2 because of fast blood clearance; however, the absolute low accumulation in the tumor (2.9% ID/g at 24 h) could compromise the sensitivity on PA images. Moreover, tumor/organ (including liver, kidneys, and muscle) ratios of HSA-ICG8.2 were the worst among all probes. There was no significant difference in T/B ratios between HSA-ICG0.5 and HSA-ICG2.9. The products of relative PA signal intensities (1, 5.6, and 13.7) multiplied by probe accumulations in the tumor (15.9, 9.5, and 2.9% ID/g) were 15.9, 53.0, and 39.3 for HSA-ICG0.5, HSA-ICG2.9, and HSA-ICG8.2, respectively. Therefore, HSA-ICG2.9 should show the highest PA signal intensity in the tumors at 24 h after injection when the same dose of HSA is administered. To obtain the same level of PA signal intensity in the tumors, a 3.3-fold injection dose is required for HSA-ICG0.5 compared to HSA-ICG2.9. Therefore, HSA-ICG2.9 was investigated for the further *in vivo* PA imaging study. The injection dose of HSA can be reduced to approximately 30% for HSA-ICG2.9 to achieve the same level of PA signal compared with HSA-ICG0.5, which can be useful for clinical translation.

3.4 *In Vivo Photoacoustic Imaging*

In vivo PA imaging was performed with HSA-ICG2.9 using the Nexus 128 system (Fig. 4). Mice were placed in the bowl as shown in Fig. 4(a). In the mice injected with HSA-ICG2.9 (13 nmol or more), the tumor was successfully visualized 24-h postinjection at 26 nmol or more [Figs. 4(c)–4(e)], while a subtle increase in the PA signal was observed in the non-tumor region [130% increase compared to preinjection for 26 nmol ICG (HSA-ICG2.9), Fig. 4(f)]. The T/M ratios calculated from *in vivo* PA images of HSA-ICG2.9 at 24 h after probe injection were 6.0 ± 2.4, 10.2 ± 2.8, 7.4 ± 2.2, and 8.9 ± 0.7 for 13, 26, 52, and 104 nmol ICG [Figs. 4(b)–4(e), respectively, which was in accordance with T/M ratios in biodistribution studies with ^{111}In-DTPA-HSA-ICG2.9 (Table 2). The PA signal in the tumor region produced by HSA-ICG2.9 increased in proportion to the ICG concentration in the range of measurement (130 ± 8, 224 ± 42, 296 ± 30, and 387 ± 37% increase compared to preinjection for 13, 26, 52, and 104-nmol ICG (HSA-ICG2.9), respectively) (Fig. 5). Furthermore, when the same dose of HSA (9 nmol) was administered, 141 ± 28, 224 ± 42, and 160 ± 5% increases in PA signals were observed for HSA-ICG0.5, HSA-ICG2.9, and HSA-ICG8.2, respectively, suggesting that HSA-ICG2.9 showed the highest sensitivity for tumor detection. The T/M ratios calculated from *in vivo* PA images at 24 h after probe injection were 14.4 ± 5.4, 10.2 ± 2.8, and 14.2 ± 1.9 for HSA-ICG0.5, HSA-ICG2.9, and HSA-ICG8.2, respectively. There was no significant difference for T/M ratios among these probes.

3.5 *Comparison between Photoacoustic Imaging and Fluorescence Imaging*

There are several reports concerning the penetration depth of the PA signal.[18,19] We also compared PA imaging with fluorescence imaging on the assumption that the tumor accumulated

Table 2 Biodistribution results for ^{111}In-DTPA-HSA-ICG or ^{111}In-DTPA-HSA in nude mice bearing subcutaneously allografted colon26 mouse rectal cancer. Results are expressed as means (%ID/g) ± SD ($n = 3 – 4$).

Organ	1 h	6 h	24 h
	HSA-ICG0.5		
Blood	31.37 ± 4.7	19.58 ± 1.41	8.51 ± 1.67
Heart	4.91 ± 1.54	4.41 ± 0.68	3.65 ± 0.65
Lungs	7.12 ± 1.19	6.05 ± 0.82	3.77 ± 0.57
Liver	8.38 ± 1.23	10.29 ± 0.66	8.86 ± 0.61
Kidneys	17.26 ± 1.12	18.78 ± 2.22	13.90 ± 1.06
Stomach	1.24 ± 0.22	1.55 ± 0.27	1.40 ± 0.04
Intestine	2.08 ± 0.24	2.66 ± 0.48	1.96 ± 0.12
Pancreas	1.54 ± 0.29	1.75 ± 0.34	2.07 ± 0.35
Spleen	5.42 ± 0.72	6.16 ± 0.41	8.57 ± 1.34
Muscle	1.00 ± 0.09	1.39 ± 0.21	1.53 ± 0.2
Tumor	3.84 ± 0.53	10.59 ± 0.91	15.88 ± 2.84
Tumor/Blood ratio	0.12 ± 0.00	0.54 ± 0.08	1.88 ± 0.15
Tumor/Muscle ratio	3.87 ± 0.59	7.67 ± 0.65	10.35 ± 1.17
	HSA-ICG2.9		
Blood	29.22 ± 3.38	15.81 ± 2.58	4.45 ± 0.78
Heart	5.52 ± 0.97	4.47 ± 0.65	3.40 ± 0.35
Lungs	7.20 ± 1.55	4.94 ± 0.4	2.99 ± 0.4
Liver	14.84 ± 1.79	24.84 ± 1.09	22.65 ± 5.21
Kidneys	9.16 ± 0.77	6.73 ± 0.3	4.76 ± 0.43
Stomach	1.29 ± 0.19	1.48 ± 0.31	0.85 ± 0.53
Intestine	1.86 ± 0.24	2.59 ± 0.25	2.14 ± 0.9
Pancreas	1.37 ± 0.19	1.33 ± 0.08	1.32 ± 0.09
Spleen	6.78 ± 0.62	8.63 ± 0.78	9.46 ± 0.97
Muscle	0.88 ± 0.2	0.96 ± 0.27	0.91 ± 0.09
Tumor	4.20 ± 0.14	8.15 ± 0.47	9.52 ± 1.58
Tumor/Blood ratio	0.14 ± 0.01	0.53 ± 0.09	2.15 ± 0.17
Tumor/Muscle ratio	4.95 ± 1.09	8.93 ± 2.07	10.63 ± 2.45
	HSA-ICG8.2		
Blood	7.62 ± 1.46	2.10 ± 0.04	0.39 ± 0.05
Heart	3.07 ± 0.65	2.09 ± 0.16	1.44 ± 0.1
Lungs	3.25 ± 0.58	1.68 ± 0.06	1.07 ± 0.14
Liver	52.33 ± 8.48	63.57 ± 1.39	49.86 ± 3.83
Kidneys	5.50 ± 1.34	3.72 ± 0.03	3.48 ± 0.34
Stomach	0.79 ± 0.33	0.56 ± 0.14	0.48 ± 0.12
Intestine	1.24 ± 0.37	1.43 ± 0.16	1.07 ± 0.12
Pancreas	0.47 ± 0.05	0.43 ± 0.01	0.49 ± 0.11
Spleen	15.42 ± 3.24	15.03 ± 0.89	12.56 ± 1.31
Muscle	0.51 ± 0.02	0.54 ± 0.28	0.55 ± 0.29
Tumor	2.37 ± 0.63	3.47 ± 0.64	2.87 ± 0.62
Tumor/Blood ratio	0.31 ± 0.04	1.65 ± 0.28	7.41 ± 2.21
Tumor/Muscle ratio	4.65 ± 1.04	8.32 ± 5.55	6.48 ± 3.25
	HSA		
Blood	32.63 ± 3.89	18.99 ± 2.26	8.40 ± 0.11
Heart	4.81 ± 0.33	4.15 ± 0.67	3.44 ± 0.28
Lungs	7.39 ± 0.24	6.27 ± 1.32	4.13 ± 0.07
Liver	10.74 ± 0.71	11.64 ± 1.89	10.42 ± 0.95
Kidneys	27.24 ± 3.09	27.00 ± 3.62	21.82 ± 0.67
Stomach	1.24 ± 0.59	1.65 ± 0.62	1.02 ± 0.25
Intestine	1.95 ± 0.25	2.71 ± 0.49	1.85 ± 0.11
Pancreas	1.44 ± 0.17	1.67 ± 0.27	1.83 ± 0.14
Spleen	5.35 ± 0.42	6.76 ± 0.97	8.04 ± 0.23
Muscle	0.91 ± 0.15	1.24 ± 0.11	1.17 ± 0.04
Tumor	4.47 ± 1.19	9.44 ± 1.86	16.79 ± 1.42
Tumor/Blood ratio	0.14 ± 0.02	0.50 ± 0.11	2.00 ± 0.18
Tumor/Muscle ratio	5.00 ± 1.48	7.62 ± 1.4	14.43 ± 1.67

HSA-ICG was located slightly deeper in the body. One-cm-thick of 1% intralipid was considered as the scattering substance of a living body.[17] The actual size of the excised tumor (0.77± 0.14 mm) was almost same as the size measured by both imaging modalities without intralipid (0.78 ± 0.15 and 0.77± 0.13 mm for fluorescence imaging and PA imaging, respectively). In the fluorescence imaging, the signal intensity in excised tumors markedly decreased (86%) and the signal area increased (1.7-fold) when covered with intralipid [Figs. 6(a) and 6(c)]. On the other hand, in the PA imaging, although the signal intensity of the tumor partially decreased (63%), the signal area was almost constant regardless of the intralipid [Figs. 6(b) and 6(c)]. The signal intensity of the PA imaging with the intralipid was significantly higher than that of fluorescence imaging [$P < 0.05$, Fig. 6(c)]. The apparent tumor size on fluorescence imaging was significantly larger than that on PA imaging [$P < 0.01$, Fig. 6(c)]. It was confirmed that PA imaging has the potential to detect tumors with a high sensitivity and resolution because of its ultrasonic characteristics.

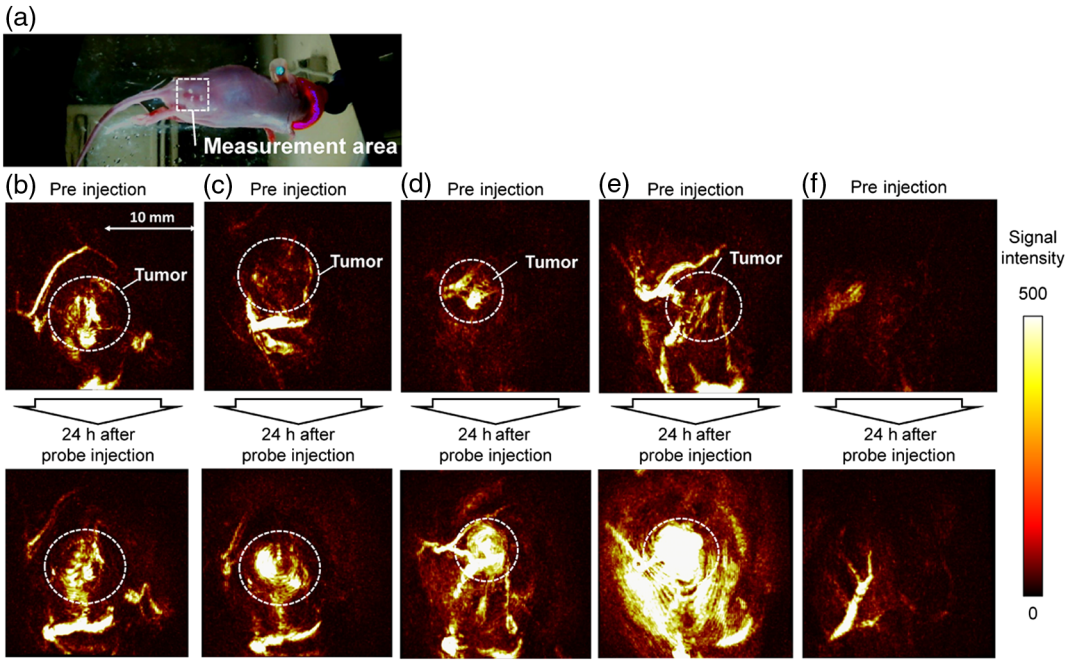

Fig. 4 PA tumor imaging with HSA-ICG2.9 in colon26 tumor-bearing mice. (a) Mouse placement in bowl. The square drawn by the dashed line was the measurement region. (b)–(f) PA images constructed with a volumetric rendering were acquired before (top) and 24 h after (bottom) tail-vein injection of 100 μL of HSA-ICG. Indocyanine green (ICG) amount of injected HSA-ICG was 13 nmol (b) and, 26 nmol (c), 52 nmol (d) and 104 nmol (e). The circles drawn by the dashed line were the tumor regions. Panels (f) are nontumor regions (leg).

4 Discussion

HSA features low immunogenicity, high biocompatibility, and good biodegradability. Because of its long circulation property, HSA is efficiently taken up by tumor tissue *via* the EPR effect, which makes it a compelling platform for molecular imaging.[14] However, an excess of HSA could induce a fall of blood pressure or the immune response,[20] and thus it is desirable to lower the injected dose of HSA-ICG to detect tumors for clinical use. In this study, the introduction of a number of ICGs (HSA-ICG8.2) compromised the tumor accumulation accompanied by a marked increase of the liver uptake. In healthy subjects, intravenously injected ICG can be taken up by the liver with a short serum half-life ($t_{1/2} = 4$ min)[21] and excreted through the biliary system without enterohepatic circulation or excretion from the kidneys.[22] This liver targeting of ICG and the slightly larger molecular weight [Fig. 1(b)] might cause an increase in the liver uptake of HSA-ICG especially for HSA with many ICGs. Moreover, the increase of size of the HSA-ICG associated with the number of ICG bound to HSA might partially cause extracellular matrix hindrance for tumor uptake. Although HSA-ICG0.5 exhibited the highest accumulation (15.9% ID/g) in the biodistribution study (Table 2), ICG-HSA2.9 was selected for *in vivo* PAI, because the injection dose of HSA can be reduced for HSA-ICG2.9 to achieve the same PA signal as for HSA-ICG0.5, which can be useful for clinical translation.

Metallic nanostructures, carbon nanotubes, and dyes have been reported as PA contrast agents.[23] Among them, single-walled carbon nanotubes conjugated with RGD peptide showed a 14% ID/g of accumulation and a 200% PA signal increase in

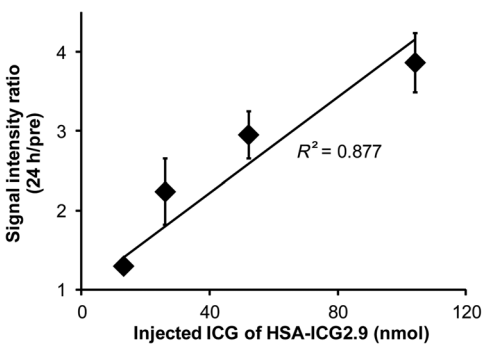

Fig. 5 The PA signal intensity ratios (24-h postinjection/preinjection) are plotted relative to the injected dose of HSA-ICG2.9. Error bars represent the standard error of measurement for the population of mice.

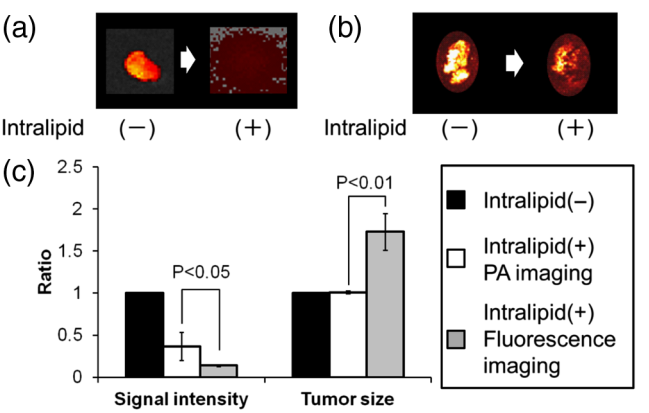

Fig. 6 Fluorescent and PA imaging of the excised tumor injected with HSA-ICG2.9. Fluorescence images (a) and PA images (b) of the tumor (left, without intralipid; right, with intralipid). (c) The change ratios of signal intensity and tumor size in the PA imaging (white) and fluorescence imaging (gray) with/without intralipid.

the tumor.[8,24] Gold nanocages with a targeting hormone showed a 40% PA signal increase in the tumor.[25] In this paper, ICG was selected as a PA signal emitter. HSA-ICG2.9 showed a 9.5% ID/g of tumor accumulation and a 380% PA signal increase for 104 nmol of HSA-ICG, yielding high-resolution deep tumor images. While ICG has a lower optical absorption ($\sim 2 \times 10^5$ cm^{-1} M^{-1}) than gold nanorods or carbon nanotubes (6×10^6 cm^{-1} M^{-1} and 10^9 cm^{-1} M^{-1}, respectively), the absorption coefficient of ICG divided by its molecular weight is greater than that of gold nanorods or carbon nanotubes (260, 35, and 0.029 cm^{-1} M^{-1} Da^{-1} for ICG, carbon nanotubes, and gold nanorods, respectively).[26] Therefore, ICG is expected to achieve a sensitive PAI at low doses, leading to the reduction of toxicity.

For PA contrast agents, it is essential to ensure patient safety and minimize risk. The safety and biocompatibility of carbon nanotubes or gold nanorods in humans remain controversial, and they have not yet gained FDA approval as *in vivo* contrast agents. Carbon nanotubes have a relatively low toxicity at 40 mg/kg, but they seem to aggregate in liver, lung, and spleen at 90 days postexposure.[27] Gold nanorods could be retained in the reticuloendothelial system (about 15% ID/g in the liver) even 14 days after injection.[28] On the other hand, HSA is FDA-approved, and the maximum permissible dose is approximately 2 g/kg per day.[29–31] Therefore, HSA has a low risk for long-term toxicity compared with carbon nanotubes or gold nanorods. In addition, ICG has also already received FDA approval and has a long track record of human use. HSA was conjugated with ICG derivatives, in which one sulfonic acid is replaced with a carbonic acid which is then used for conjugation, without altering the cyanine structure important for NIR absorption. Formal safety studies of the final conjugates will be required prior to approval for human use, but it is encouraging that each component has a favorable toxicity profile.

Fluorescence imaging, one of the noninvasive imaging methods other than PAI, has high sensitivity and instantaneousness. However, the fluorescence of ICG can be quenched based on hetero-FRET (fluorescence resonance energy transfer)[32–34] when bound to proteins such as antibodies. The signal might be changed by surrounding environment (concentration of the probe, depth from the surface). The quenching capacity can be increased as the number of ICG bound to HSA increased. Therefore, *in vivo* fluorescence intensity in the body (tumor) can be estimated to be lower compared with the radiolabeled experiment, especially at an early time point after injection for HSA-ICG8.2. In fact, our data showed the same level of fluorescence signal in the tumor (24-h post-injection) even if the amounts of tumor accumulation differed [Figs. 3(a), 3(b), and 3(d)]. On the other hand, PAI can provide more quantitative images than fluorescence imaging as shown in Figs. 4 and 5. Increasing the dose of the HSA-ICG2.9 by twofold increments did not necessarily increase the PA signal by increments of x2 ($R^2 = 0.88$). This is probably because the laser was nonuniformly irradiated to the tumors, which might be dependent on the position of the tumors. Furthermore, PAI using HSA-ICG allows us to identify more deeply seated tumors, as shown in Fig. 6, based on the stronger penetration properties of ICG with an excitation wavelength >700 nm and ultrasonic waves which are scattered much less than photons, which is superior to fluorescence imaging.

In conclusion, HSA-ICG can provide clear images of allografted tumors with high tumor-to-background ratios, high quantitivity, and spatial resolution. Because both HSA and ICG have already been approved by the FDA, there is a high possibility of clinical translation of HSA-ICG as a PA contrast agent.

Acknowledgments

This work was partly supported by the Innovative Techno-Hub for Integrated Medical Bio-imaging Project of the Special Coordination Funds for Promoting Science and Technology, from the Ministry of Education, Culture, Sports, Science and Technology (MEXT), Japan.

References

1. D. Razansky et al., "Deep tissue optical and optoacoustic molecular imaging technologies for pre-clinical research and drug discovery," *Curr. Pharm. Biotechnol.* **13**(4), 504–522 (2012).
2. V. Ntziachristos, "Going deeper than microscopy: the optical imaging frontier in biology," *Nat. Methods.* **7**(8), 603–614 (2010).
3. J. Laufer et al., "*In vivo* preclinical photoacoustic imaging of tumor vasculature development and therapy," *J. Biomed. Opt.* **17**(5), 056016 (2012).
4. G. P. Luke, D. Yeager, and S. Y. Emelianov, "Biomedical applications of photoacoustic imaging with exogenous contrast agents," *Ann. Biomed. Eng.* **40**(2), 422–437 (2012).
5. G. Ku and L. V. Wang, "Deeply penetrating photoacoustic tomography in biological tissues enhanced with an optical contrast agent," *Opt. Lett.* **30**(5), 507–509 (2005).
6. W. J. Akers et al., "Multimodal sentinel lymph node mapping with single-photon emission computed tomography (SPECT)/computed tomography (CT) and photoacoustic tomography," *Transl. Res.* **159**(3), 175–181 (2012).
7. D. Pan et al., "Near infrared photoacoustic detection of sentinel lymph nodes with gold nanobeacons," *Biomaterials* **31**(14), 4088–4093 (2010).
8. A. de la Zerda et al., "Family of enhanced photoacoustic imaging agents for high-sensitivity and multiplexing studies in living mice," *ACS Nano* **6**(6), 4694–4701 (2012).
9. G. Kim et al., "Indocyanine-green-embedded PEBBLEs as a contrast agent for photoacoustic imaging," *J. Biomed. Opt.* **12**(4), 044020 (2007).
10. J. V. Frangioni, "*In vivo* near-infrared fluorescence imaging," *Curr. Opin. Chem. Biol.* **7**(5), 626–634 (2003).
11. V. L. Dzurinko, A. S. Gurwood, and J. R. Price, "Intravenous and indocyanine green angiography," *Optometry* **75**(12), 743–755 (2004).
12. S. G. Sakka, "Assessing liver function," *Curr. Opin. Crit. Care* **13**(2), 207–214 (2007).
13. Y. Ishima et al., "S-Nitrosated human serum albumin dimer is not only a novel anti-tumor drug but also a potentiator for anti-tumor drugs with augmented EPR effects," *Bioconjug. Chem.* **23**(2), 264–271 (2012).
14. B. Elsadek and F. Kratz "Impact of albumin on drug delivery—new applications on the horizon," *J. Control. Release* **157**(1), 4–28 (2012).
15. H. Maeda, "Tumor-selective delivery of macromolecular drugs *via* the EPR effect: background and future prospects," *Bioconjug. Chem.* **21**(5), 797–802 (2010).
16. H. Maeda and Y. Matsumura, "EPR effect based drug design and clinical outlook for enhanced cancer chemotherapy," *Adv. Drug Deliv. Rev.* **63**(3), 129–130 (2011).
17. J. R. Cook, R. R. Bouchard, and S. Y. Emelianov, "Tissue-mimicking phantoms for photoacoustic and ultrasonic imaging," *Biomed. Opt. Express* **2**(11), 3193–3206 (2011).
18. A. Krumholz et al., "Multicontrast photoacoustic in vivo imaging using near-infrared fluorescent proteins," *Sci. Rep.* **4**, 3939 (2014).
19. Y. Wang and L. V. Wang, "Förster resonance energy transfer photoacoustic microscopy," *J. Biomed. Opt.* **17**(8), 086007 (2012).
20. T. W. Evans, "Review article: albumin as a drug—biological effects of albumin unrelated to oncotic pressure," *Aliment. Pharmacol. Ther.* **16**(Suppl 5), 6–11 (2002).
21. G. R. Cherrick et al., "Indocyanine green: observations on its physical properties, plasma decay, and hepatic extraction," *J. Clin. Invest.* **39**(4), 592–600 (1960).

22. C. A. Dawson et al., "Influence of plasma protein on the inhibitory effects of indocyanine green and bromcresol green on pulmonary prostaglandin E1 extraction," *Br. J. Pharmacol.* **81**(3), 449–455 (1984).
23. M. Mehrmohammadi et al., "Photoacoustic imaging for cancer detection and staging," *Curr. Mol. Imag.* **2**(1), 89–105 (2013).
24. Z. Liu et al.," *In vivo* biodistribution and highly efficient tumour targeting of carbon nanotubes in mice," *Nat. Nanotechnol.* **2**(1), 47–52 (2007).
25. C. Kim et al.," *In vivo* molecular photoacoustic tomography of melanomas targeted by bioconjugated gold nanocages," *ACS Nano* **4**(8), 4559–4564 (2010).
26. A. de la Zerda et al., "Advanced contrast nanoagents for photoacoustic molecular imaging, cytometry, blood test and photothermal theranostics," *Contrast Media Mol. Imaging* **6**(5), 346–369 (2011).
27. S. T. Yang et al., "Long-term accumulation and low toxicity of single-walled carbon nanotubes in intravenously exposed mice," *Toxicol. Lett.* **181**(3), 182–189 (2008).
28. L. Nie et al., "*In vivo* volumetric photoacoustic molecular angiography and therapeutic monitoring with targeted plasmonic nanostars," *Small* **10**(8), 1585–1593 (2014).
29. J. L. Tullis, "Albumin. 2. Guidelines for clinical use," *J. Am. Med. Assoc.* **237**(5), 460–463 (1977).
30. L. C. Vermeulen, Jr. et al., "A paradigm for consensus. The University Hospital Consortium guidelines for the use of albumin, nonprotein colloid, and crystalloid solutions," *Arch. Int. Med.* **155**(4), 373–379 (1995).
31. C. M. Mendez, C. J. McClain, and L. S. Marsano, "Albumin therapy in clinical practice," *Nutr. Clin. Pract.* **20**(3), 314–320 (2005).
32. K. Sano et al.," In vivo breast cancer characterization imaging using two monoclonal antibodies activatably labeled with near infrared fluorophores," *Breast Cancer Res.* **14**(2), R61 (2012).
33. K. Sano et al., "Short PEG-linkers improve the performance of targeted, activatable monoclonal antibody-indocyanine green optical imaging probes," *Bioconjugate Chem.* **24**(5), 811–816 (2013).
34. K. Sano et al., "Activatable fluorescent cys-diabody conjugated with indocyanine green derivative: consideration of fluorescent catabolite kinetics on molecular imaging," *J. Biomed. Opt.* **18**(10), 101304 (2013).

Biographies of the authors are not available.